

MXenes à la Carte: Tailoring the Epitaxial Growth Alternating Nitrogen and Transition Metal Layers

José D. Gouveia,^{‡,¶} Ángel Morales-García,^{†,¶} Francesc Viñes,^{*,†} José R. B. Gomes,[‡]
Francesc Illas[†]

[†]*Departament de Ciència de Materials i Química Física & Institut de Química Teòrica i Computacional (IQTCUB), Universitat de Barcelona, c/ Martí i Franquès 1-11, 08028 Barcelona, Spain*

[‡]*CICECO – Aveiro Institute of Materials, Department of Chemistry, University of Aveiro, Campus Universitário de Santiago, 3810-193 Aveiro, Portugal*

* Corresponding author: Francesc Viñes (francesc.vines@ub.edu)

ABSTRACT

A high-throughput analysis based on density functional simulations underscores the viable epitaxial growth of MXenes by alternating nitrogen and metal adlayers. This is supported by an exhaustive analysis of a number of thermodynamic and kinetic thresholds belonging to different critical key steps in the course of the epitaxial growth. The results on 18 pristine N- and C-based MXenes with M_2X stoichiometry reveal an easy initial N_2 fixation and dissociation, where N_2 adsorption is controlled by the MXene surface charge and metal d -band center, and its dissociation controlled by the reaction energy change. Furthermore, formation energies indicate the plausible formation of N-terminated M_2XN_2 MXenes. Aside, the further covering with metal adlayers is found to be thermodynamically driven and stable, especially when using early transition metal atoms. The most restrictive analyzed criterion is the N_2 adsorption and dissociation at nearly full N-covered adlayers, yet achievable for almost half of the explored M_2X seeds. The present results unfold the possibility of expanding, controlling and tuning the composition, width, and structure of the MXenes family.

Keywords: MXenes, epitaxial growth, density functional simulations, thermodynamics, kinetics

[¶]These authors contributed equally.

1. Introduction

MXenes are novel two-dimensional (2D) materials¹ which lately have attracted a considerable amount of attention because of their blooming possible technological uses in a large number of fields,² ranging from adequate substrates for future new generations of lithium-based batteries,³ to effective materials for electromagnetic interference (EMI) shielding,⁴ and suited substrates for carbon dioxide (CO₂) capture,⁵⁻⁷ a key issue in the quest of fighting global warming. Furthermore, many research endeavors have put MXenes under the spotlight as sensors for organic or biological compounds,⁸⁻¹⁰ up to the point that MXene-graphene composites have been pointed out as low-cost, ultrasensitive, and fast-responding sensors for the H1N1 influenza virus and SARS-CoV-2 coronavirus.¹¹

All the above MXene uses highly depend on their composition, geometry, and surface termination. Most MXenes can be classified as 2D few-layered transition metal carbides and nitrides with $M_{n+1}X_n$ formula, n defining the thickness of MXene, with normally $n = 1-3$, although $n = 4$ MXenes, such as Mo_4VC_4 ,¹² have been synthesized and characterized, and there are reports of trace impurities of MAX phases with larger n , such as Ta_6AlC_5 and Ti_7SnC_6 .^{13,14} The M component is generally an early transition metal, typically from groups III-VI of the Periodic Table, while X is either C or N. This already generates a large pool of combinatorial possibilities, but the family size is further increased when accounting for carbonitride MXenes,¹⁵ as well as bimetallic MXenes, either in the form of layered solid solutions (*i*-MXenes) or displaying some degree of layered ordering (*o*-MXenes).¹⁶

Additionally, one has to account for the MXene surface terminations, generally denoted as T_x , resulting from the MXene synthesis protocol, which considerably enlarge the aforementioned pool of possibilities. MXenes are generally attainable by selective chemical etching of the A element of MAX phases, usually employing hydrofluoric acid (HF) for such a purpose,¹ followed by sonication to separate the MXene layers, although the use of lithium fluoride (LiF) and hydrochloric acid (HCl) to generate *in situ* HF has been gaining momentum.¹⁷ This treatment generally leaves the MXene surface terminated by a combination of hydrogen (H), oxygen (O), hydroxyl (OH), and fluorine (F) groups for a variety of working conditions,^{18,19} despite diverse fluorine-free synthesis procedures having been proposed, so as to control the surface termination variable and ease the preparation process.^{20,21}

Last but not least, there have been recent advances showing that pristine MXenes, *i.e.* with no surface terminations, can be gained, either from a T_x -containing one, removing the T_x after hydrogenation and annealing protocols,⁷ or directly synthesized departing from halide-terminated MXenes.²² All in all, the MXene family is vast and quickly growing. However, their number is quite restricted to the availability of a suited MAX phase —over 155 so far reported and growing, including some $n > 3$ materials.²³ Within this context, apart from grinding synthetic methods, one has to highlight the possibility of gaining MAX thin films epitaxially grown on a given support, such as sapphire Al_2O_3 , by magnetron sputtering,^{24,25} with reports revealing the synthesis of bimetallic alloy MAX phases such as $(Ti,Zr)AlC_2$,²⁶ or the Ge-based $Ti_{n+1}GeC_n$ ($n = 1-3$) family.²⁷

Spurred by these previous findings, a (still open) question arises: Would it be feasible to directly epitaxially grow MXenes, even to go for $n > 3$? To answer this question, one must obviously regard the recently experimentally gained pristine MXenes,^{7,22} as the surface T_x would act as a passivator layer. Within this frame, it has been shown, by means of density functional theory (DFT) computational studies, that pristine M_2X MXenes — $M = Ti, Zr, Hf, V, Nb, Ta, Cr, Mo, W$; $X = C$ or N — are quite capable of chemically adsorbing nitrogen (N_2), with adsorption energies, E_{ads} , ranging from -1.11 to -3.45 eV, and dissociating it, with N_2 dissociation energy barriers, E_b , between 0.28 and 1.10 eV.²⁸ Aside, there exist metal chemical vapor deposition (CVD) methods to create early M films, mostly using a transition metal halide or complex as precursor.²⁹ In particular, MBr_4 and MCl_4 compounds have been used to generate Cl- or Br-terminated MXenes and, given the weak M-halide bond, these have been used to obtain pristine MXenes as well as a large variety of additional T_x terminations ($T_x = O, S, NH, Se, Te$).²²

With the information provided above, one could envisage a process in which a pristine MXene M_2X seed material is used to capture and decompose N_2 , ideally eventually gaining a fully N-covered M_2XN_2 MXene surface, and that this could, in turn, be used as well as a substrate to deposit M' layers on-top, resulting in $M'_2M_2XN_2$ compounds, where M' could be, in principle, any early transition metal compound. Lastly, by combining these processes, one would effectively epitaxially grow the MXene compound while controlling the composition of the outer layers. Hereby we demonstrate, by DFT-based modeling on a series of MXene systems, that such epitaxial growth is attainable for several MXene seeds, meeting a number of thermodynamic and kinetic thresholds, and paving the way for tailor-making MXenes with a controlled surface metal M and X ending.

2. Methods and Models

A set of MXene seeds with M_2X formula has been studied, including M elements from groups IV (Ti, Zr, Hf), V (V, Nb, Ta), and VI (Cr, Mo, W), while $X = C$ or N, totaling 18 M_2X MXenes. Their basal (0001) surfaces have been described through $p(3\times 3)$ supercell slab systems, as done in former studies.^{6,30,31} In all calculations, the MXene atomic positions as well as those of adsorbate atoms or molecules were fully optimized by total energy minimization. The employed supercells have a vacuum length along the (0001) basal cell vector of at least 10 Å, enough to practically nullify the interactions among replicated slabs or the adsorbates. Notice that M_2X , M_2XN_2 , and $M'_2M_2XN_2$ MXenes unit cells were fully optimized prior to adsorbing either metal atoms thereon, or adsorbing and dissociating a N_2 molecule.

One aspect to be regarded is that M_2X MXene seeds do not necessarily have to feature the ABC atomic layer stacking of the parent MAX phases, as recent studies revealed that ABA stacking is thermodynamically preferred and kinetically achievable for some MXenes. Indeed, the ABA preference is fostered by the number of the d electrons of the M element, when having $X = N$ instead of C, and when $T_x = O$.³² Furthermore, in this previous computational study, it was emphasized that stacking could have an impact on the surface chemical activity, evaluated for the N_2 adsorption and dissociation, with changes up to ~ 1 eV for E_{ads} , and up to 0.3 eV for E_b . Accordingly, in this work, the most stable stacking was used in each M_2X seed, and a stacking energetic preference study was conducted for the N-terminated cases, *i.e.* M_2XN_2 .

The present first-principles based analysis was carried out using the Vienna *ab initio* simulation package (VASP).³³ In order to compare the present results with previous studies on N_2 adsorption and dissociation on M_2X (0001) surfaces,^{28,32} the Perdew-Burke-Ernzerhof (PBE) exchange-correlation functional,³⁴ combined with the Grimme D3 treatment of dispersive forces,³⁵ was employed. Projector augmented wave (PAW) pseudopotentials were used to describe the effect of core electrons on the valence electron density.³⁶ The latter was expanded in a plane wave basis set with a maximum kinetic energy cut-off of 415 eV. The Brillouin zone integration was sampled using optimal Monkhorst-Pack \mathbf{k} -grids of $5\times 5\times 1$ dimensions.³⁷ The threshold for the electronic optimization has been set to 10^{-5} eV, and geometry optimizations were considered finished when forces acting on atoms were below 0.01 eV Å⁻¹. Notice that test calculations using more stringent values for kinetic energy cutoff, \mathbf{k} -points mesh, or the

thresholds used as optimization criteria yielded variations in computed E_{ads} below chemical accuracy, *i.e.* below ~ 0.04 eV ~ 1 kcal \cdot mol $^{-1}$. All calculations were carried out accounting for spin polarization unless stated otherwise. Still, test calculations on $p(1\times 1)$ unit cells considering non-magnetic, ferromagnetic, and antiferromagnetic solutions confirmed that the energy difference between the different magnetic configurations is almost negligible for M_2X seeds, with no magnetization found neither for M_2XN_2 , nor for $M'_2M_2XN_2$ materials, see Table S1 of the Supporting Information (SI). To evaluate the stability of the epitaxially grown materials, N_2 in vacuum and bulk metal references were taken as references. The geometry of the isolated N_2 molecule in its closed shell electronic ground state was optimized using the PBE-D3 functional at Γ -point in an asymmetric cell of $9\times 10\times 11$ Å, as previously done in the literature.²⁸ Bulk metals were optimized as done and available in the literature.³⁸⁻⁴⁰

The search for the adsorbed N_2 dissociation transitions states (TSs) was carried out by means of either the climbing-image nudged elastic band (CI-NEB) method,⁴¹ or the dimer⁴² methods. All stationary points, that is, the found minima and TSs, were properly characterized through a pertinent vibrational frequency analysis, where frequencies were calculated only for the adsorbate, and hence, decoupled from the substrate phonons. To estimate the frequencies, the corresponding block of the Hessian matrix was built through finite differences of analytical gradients with displacements of 0.015 Å. The resulting matrix was diagonalized, and the so-gained eigenvalues correspond to the frequencies of the normal vibrational modes. All minima and TSs featured none or just one imaginary frequency, respectively.

3. Decalogue of Suitability

In order to rationalize the suitability of epitaxially growing MXenes in terms of thermodynamic and kinetic stability, a list of ten criteria was defined, as disclosed below, following natural steps to be successively met in the course of the epitaxial growth; for instance, N_2 has to chemically adsorb on the studied M_2X MXene seed prior to its molecular dissociation. Thus, epitaxial growth is likely to happen when the ten criteria are met in succession, although all criteria have been examined for all the cases. This was not done just for completeness, but also as one could envisage alternative paths to ensure accomplishing one unmet criterion, which acts as a pebble-in-the-shoe in the epitaxial growth; for instance, we consider N_2 as the N source, but it could well be ammonia, pyridine or pyrrole, to name a few. The goal of this evaluation is thus to provide a

roadmap on the epitaxial growth, although secondary paths are not excluded from the equation.

The ten criteria are as follow, so, for a given M_2X to be a likely good seed for epitaxial growth, it must display:

i) a thermodynamically favorable N_2 adsorption on pristine M_2X . For this, the N_2 adsorption energy, $E_{\text{ads}}^{N_2}$, is defined as

$$E_{\text{ads}}^{N_2} = E_{N_2/M_2X} - E_{M_2X} - E_{N_2} + \Delta E_{\text{ZPE}} \quad (1),$$

where E_{N_2/M_2X} is the total energy of the M_2X MXene with an N_2 molecule adsorbed on one of its (0001) surfaces, E_{M_2X} is the total energy of the corresponding M_2X pristine MXene, and E_{N_2} is the energy of the isolated N_2 molecule. The ΔE_{ZPE} term is the difference in zero-point energy (ZPE) of the N_2 in gas phase or when adsorbed. According to this definition, a favorable adsorption implies negative $E_{\text{ads}}^{N_2}$ values, and hence, the more negative, the stronger the adsorption is. Note that, for N_2 in vacuum, there is only one vibrational frequency, related to the N_2 bond stretching. However, when adsorbed, the linear symmetry is broken and the rotational and translation normal modes become frustrated due to the bonding of N_2 molecule to the MXene substrate. Therefore, the number of normal vibrational modes of the adsorbed species becomes six. That considered, the ZPE for gas phase species or when adsorbed are calculated as

$$E_{N_2,\text{vac}}^{\text{ZPE}} = \frac{1}{2} \hbar \omega \quad (2),$$

$$E_{N_2,\text{ads}}^{\text{ZPE}} = \frac{1}{2} \sum_{i=1}^6 \hbar \omega_i \quad (3),$$

respectively, where \hbar is the reduced Planck constant, and ω_i are the vibrational angular frequencies. Thus, the ZPE term is simply

$$\Delta E_{\text{ZPE}} = E_{N_2,\text{ads}}^{\text{ZPE}} - E_{N_2,\text{vac}}^{\text{ZPE}} \quad (4).$$

ii) a kinetic preference towards N_2 dissociation compared to the N_2 desorption. In this regard, the N_2 dissociation energy barrier on the pristine M_2X MXene seed (0001) surface, $E_b^{N_2}$, should be by default smaller than the N_2 molecular desorption energy, $E_{\text{des}}^{N_2}$, here defined as the symmetric of the adsorption energy, *i.e.* $E_{\text{des}}^{N_2} = -E_{\text{ads}}^{N_2}$, succinctly implying that dissociation is easier than desorption.

iii) *an energetic preference towards N₂ dissociation.* This is, the N₂ dissociation reaction step energy difference, $\Delta E_{\text{dis}}^{\text{N}_2}$, calculated as the energy difference between the final dissociated state containing two vicinal N adatoms and the initial state having the adsorbed N₂ molecule, has to be clearly exothermic, implying that there is a tendency towards its dissociation rather than towards the recombination of the two N adatoms into adsorbed N₂.

So far, criteria *i-iii*) would define the likeliness of pristine M₂X MXenes in capturing and breaking a N₂ molecule, eventually having a MXene with two vicinal N adatoms, *i.e.* having MXenes with an N-adatom surface coverage, θ_{N} , of $2/9$ monolayers (ML), where the number 2 is due to the dissociated N₂ molecule, and 9 is the number of active sites in our $p(3 \times 3)$ MXene supercell model, equal to the number of atoms on each of the MXene exposed surfaces. The next criteria evaluate these and other aspects for the same process, but so as to eventually obtain an M₂X MXene with full N-adatom coverage, *i.e.* $\theta_{\text{N}} = 1$ ML. To this end, a full N-coverage situation was designed for each studied M₂X, acquiring and optimizing the atomic structure of M₂XN₂ models, departing, as aforementioned, from most stable stacking situations. The stability of the resulting M₂XN₂ MXenes was further analyzed, beyond ABC and ABA stacking, in order to find the most stable minimum, implying, in some cases, different N-terminations, *e.g.* an NMXMN stacking following a BABCA sequence, as found on Ti₂CN₂, where both surface N layers have different environment; *i.e.* being aligned with the central X layer, or with the farthest M layer. Such cases are Janus MXenes by definition,^{43,44} where both surface endings are different. In such cases, the following criteria were evaluated on each surface ending. Thus, once the structure is optimized, two vicinal N adatoms are removed and the structure reoptimized, so that a model with $\theta_{\text{N}} = 7/9$ ML is created. For a favorable epitaxial growth, these models must display:

iv) *a thermodynamically favorable N₂ adsorption.*

v) *a kinetic preference towards N₂ dissociation compared to N₂ desorption.*

vi) *an energetic preference towards N₂ dissociation.*

These are the same as criteria *i-iii*), but for a nearly full N-coverage, altogether fringing the limits of a full monolayer creation, *i.e.* kinetically and energetically suitable from its first stage up to the final full-coverage situation. Further than that, the as-created M₂XN₂ MXene must have

vii) *a suitable formation energy for M_2XN_2 .* To this end, the formation energy, E_{form} , is defined as

$$E_{\text{form}} = E_{M_2XN_2} - E_{M_2X} - E_{N_2} \quad (5),$$

where $E_{M_2XN_2}$ is the energy of the optimal M_2XN_2 MXene, and the E_{form} values obtained are given per formula unit. In this context, a suitable formation energy must be negative, implying that the formation of M_2XN_2 is exothermic and thermodynamically driven.

Finally, on the so-gained M_2XN_2 , one may adsorb a single early transition metal M' atom from groups IV-VI, with $\theta_{M'} = 1/9$ ML, and also envision a full-coverage situation, $\theta_{M'} = 9/9$ ML, in which such atoms occupy most stable positions on the surface —or on each surface in case of Janus M_2XN_2 models. In the latter case, the atomic structure of the resulting $M_2'M_2XN_2$ MXene is again fully optimized, and on such a model, an M' atom is removed and the system structure re-optimized, so as to have a nearly full M' surface situation, $\theta_{M'} = 8/9$ ML. On these models, one has to evaluate whether M_2XN_2 is suited for an epitaxial growth, as they must display:

viii) *a viable metal adatom adsorption energy on pristine M_2XN_2 .* In this sense, the metal adatom adsorption energy, $E_{\text{ads}}^{M'}$, is calculated as

$$E_{\text{ads}}^{M'} = E_{M'/M_2XN_2} - E_{M_2XN_2} - E_{\text{bulk}}^{M'} \quad (6),$$

where E_{M'/M_2XN_2} is the energy of the M_2XN_2 model with one M' adatom adsorbed, and $E_{\text{ads}}^{M'}$ is the bulk energy of a single M' atom. Notice that bulk energies had already been obtained in earlier DFT studies using the same computational setup.³⁸⁻⁴⁰ Within this definition, a negative $E_{\text{ads}}^{M'}$ value implies that the single atom is energetically more comfortable as an adatom on the M_2XN_2 model than in its pure M' bulk environment, a thermodynamic assessment that has long been used in seizing the single-atom surface thermodynamic stability on 2D materials.⁴⁵⁻⁴⁷ Note that this criterion is more stringent than when the energy of the M' atom is assumed to be the energy of the isolated M' atom in vacuum.

ix) *a viable metal adatom adsorption energy to form $M_2'M_2XN_2$.* This is, a negative $E_{\text{ads}}^{M'}$ value when adsorbed on the $\theta_{M'} = 8/9$ ML $M_2'M_2XN_2$ model; in other words, on the M' surface vacancy of the otherwise fully M' covered $M_2'M_2XN_2$ model. This threshold implies that such a full metal monolayer is thermodynamically driven. This adsorption energy is obtained as

$$E_{\text{ads}}^{\text{M}'} = E_{\text{M}'/\text{M}'_{2-x}\text{M}_2\text{XN}_2} - E_{\text{M}'_{2-x}\text{M}_2\text{XN}_2} - E_{\text{bulk}}^{\text{M}'} \quad (7),$$

where $E_{\text{M}'_{2-x}\text{M}_2\text{XN}_2}$ is the energy of a $\theta_{\text{M}'} = 8/9$ ML $\text{M}'_2\text{M}_2\text{XN}_2$ model, and $E_{\text{M}'/\text{M}'_{2-x}\text{M}_2\text{XN}_2}$ the energy of a $\theta_{\text{M}'} = 1$ ML $\text{M}'_2\text{M}_2\text{XN}_2$ model.

x) a suitable formation energy for $\text{M}'_2\text{M}_2\text{XN}_2$. To this end, the $\text{M}'_2\text{M}_2\text{XN}_2$ formation energy is calculated as

$$E_{\text{form}} = E_{\text{M}'_2\text{M}_2\text{XN}_2} - E_{\text{M}_2\text{XN}_2} - 2 \cdot E_{\text{bulk}}^{\text{M}'} \quad (8),$$

where $E_{\text{M}'/\text{M}'_2\text{M}_2\text{XN}_2}$ is the energy of a $\theta_{\text{M}'} = 1$ ML $\text{M}'_2\text{M}_2\text{XN}_2$ model, and given per $\text{M}'_2\text{M}_2\text{XN}_2$ formula unit. Thus, a negative E_{form} would imply that the formation of $\text{M}'_2\text{M}_2\text{XN}_2$ from bulk M' and M_2XN_2 would be exothermic, and thermodynamically favourable. Thus, criteria *viii-x)* define whether the formation of M' adlayers is thermodynamically driven.

4. Results and Discussion

Having defined the decalogue of conditions enabling an epitaxial growth of alternating N and M' layers on an M_2X MXene seed, we analyze them one at a time in this section. Let us begin with the N_2 molecule adsorption energy on the pristine M_2X (0001) surface models. The computed adsorption energies for all the models have been collected from the literature,^{28,32} taking into account the most preferred M_2X layers stacking. For convenience, the $E_{\text{ads}}^{\text{N}_2}$ values are listed in Table S2 of the SI. The casuistry of this criterion is graphically summarized in Figure 1, assuming that any negative $E_{\text{ads}}^{\text{N}_2}$ value is favorable, and, *vice versa*, that any positive $E_{\text{ads}}^{\text{N}_2}$ value is unfavorable. Given the standard DFT accuracy of ± 0.2 eV, *i.e.* assuming that $E_{\text{ads}}^{\text{N}_2}$ values may vary by this amount when using another exchange-correlation functional and/or estimate of dispersive forces correction, $E_{\text{ads}}^{\text{N}_2}$ values of ± 0.2 eV are taken with a grain of salt, and considered dubious. In the present situation, notice that, since $E_{\text{ads}}^{\text{N}_2}$ values range from -1.14 (W_2C) to -3.45 eV (Ti_2N), in all cases indicating a strong chemisorption, all the M_2X seed accomplish this first criterion. As can be seen in Figure S1 of the SI, the $E_{\text{ads}}^{\text{N}_2}$ values on pristine M_2X models seem to correlate with both the surface metal *d*-band center, ε_a , and the surface metal charge, ΔQ_m , with regression coefficients, *R*, of 0.76 and 0.83, respectively, and so, governed by the same factor that determines CO_2 and CO adsorption strengths, as previously reported.⁴⁸

The second criterion is that the dissociation energy barrier for the adsorbed N_2 , $E_b^{N_2}$, must be smaller than the desorption energy, here defined as $-E_{ads}^{N_2}$. Table S2 of the SI collects the computed $E_b^{N_2}$ values from the literature,^{28,32} ranging from 0.18 (W₂N) to 1.1 eV (Zr₂C). Even considering the most detrimental error thresholds due to the DFT accuracy, that is, $E_{ads}^{N_2}$ values systematically overestimated, and $E_b^{N_2}$ values systematically underestimated, the difference between the estimated $E_{ads}^{N_2}$ and $E_b^{N_2}$ values is large, at least of 0.74 eV for Mo₂C, implying that this criterion is accomplished for all the investigated M₂X MXenes; see Figure 1. Finally, the third criterion for the pristine M₂X seeds is that the N_2 dissociation reaction step energy difference, $\Delta E_{dis}^{N_2}$, should be negative (exothermic). The values, taken again from the literature,^{28,32} and encompassed in Table S2 of the SI, and are all negative, ranging from -1.55 (Ti₂C) to -3.22 eV (W₂N). Thus, even when accounting for DFT accuracy, all the explored MXenes accomplish this last criterion, as seen in Figure 1.

As a representative example, Figure 2 depicts the reaction profile for the N_2 adsorption and dissociation steps on the Ta₂C (0001) model. Notice here how the $E_{ads}^{N_2}$ of -2.35 eV is clearly larger in magnitude than the N_2 dissociation energy barrier, $E_b^{N_2}$, of 0.53 eV. Finally, the N_2 dissociation elementary step implies a favorable energy reduction, $\Delta E_{dis}^{N_2}$, of -2.72 eV. Thus, all of the first three criteria of the decalogue are met. Notice that the $E_b^{N_2}$ and $\Delta E_{dis}^{N_2}$ values follow a clear Brønsted-Evans-Polanyi (BEP) relationship, including to this end high-coverage situations, see below and Figure S2 of the SI, with a regression coefficient, R, of 0.96, and a mean absolute error on predicted $E_b^{N_2}$ of solely 0.3 eV, close to the aforementioned DFT accuracy.

Further than this, we evaluated the working conditions at which N adatom moieties, N*, are kinetically preferred to be located at the Ta₂C (0001) surface. Accordingly, adsorption/desorption rates, as well as N_2 dissociation and 2N recombination rates have been estimated as a function of temperature, T , and N_2 partial pressure, p_{N_2} . Briefly, collision theory was used for the adsorption rate, while transition state theory (TST) was used for the rest of the reaction elementary steps, using a N_2 sticking coefficient similar to that of N_2 on Pt surfaces, of 0.68,⁴⁹ also justified by the similar behavior of early transition metal carbides to Pt-group elements.⁵⁰ Aside, a rotational temperature of 2.88 K was employed for N_2 in vacuum, as taken from the literature,⁵¹ while nine adsorption

sites are considered on each exposed MXene surface area. For more details on the mathematical framework and procedure, we refer the reader to the literature.⁴⁸

Figure 3 shows the different elementary reaction step rates and the built kinetic phase diagram, where a solid line denotes the equilibrium conditions where $r_{\text{ads}} = r_{\text{des}}$, so that for T and p_{N_2} values under the line, the desorption process is preferred over the adsorption one, and the system would have a preference towards being clean, *i.e.* absent of adsorbed atomic or molecular moieties.⁵² On the other hand, for p_{N_2} and T conditions above the equilibrium line, the N_2 adsorption rate, r_{ads} , is larger than the desorption rate, r_{des} , implying a preferential accumulation of N_2 on the Ta_2C (0001) surface. Moreover, within this region, the molecularly adsorbed N_2 , N_2^* , dissociation rate, r_{dis} , is always larger than the 2N recombination rate, r_{rec} , and so N^* adatoms are envisioned as the kinetically driven surface species. All in all, N_2 adsorption and dissociation seems quite feasible on the Ta_2C (0001) selected model, as well as on other studied MXenes. For instance, on Ta_2C , and with N_2 at standard pressure; $p_{\text{N}_2} = 1$ bar, one could start accumulating N^* moieties at working temperature below the 1000 K explored limit. However, one should regard that such conditions are suited for the initial stages of N covering, but such conditions may change for larger θ_{N} , *vide infra*.

Accordingly, we next explored the fully N-covered M_2X , *i.e.* M_2XN_2 models. The structural optimizations considering different possible stacking options revealed that, similarly to the previous observations on O-terminated MXenes,³² the group VI (Cr_2X , Mo_2X , and W_2X) MXenes featured a thermodynamic preference towards ABA stacking, see difference in energy of ABA vs. ABC per formula unit, ΔE_{stack} , in Figure 4, and values in Table S3 of the SI. Notice that, compared to the case of O-termination, the N-termination still favors ABA stacking, but by a smaller energy difference, this is, ΔE_{stack} values ranging from -0.21 (W_2CN_2) to -0.56 eV (Mo_2N_3), significantly smaller when compared to the values of -1.05 (Cr_2CO_2) to -2.33 eV (W_2CO_2), as reported in previous work.³²

Aside from the previously stated, the N-termination does not necessarily have to follow the stacking trend. For instance, structural optimizations revealed a different surface ending for group IV carbon-based MXenes (Ti_2C , Zr_2C , Hf_2C), where the N surface termination layers occupy different surface sites on each face of the material; in particular, adsorbed on a Hollow site aligned with a metal atom lying three layers underneath (H_M), or adsorbed on a Hollow site but aligned with a C atom two layers

underneath (H_C). This means that Ti_2CN_2 , Zr_2CN_2 , and Hf_2CN_2 models are actually Janus MXenes, with different surface terminations, and, consequently, each one was explored separately. A similar situation occurs for Cr_2CN_2 , but here, given the ABA stacking of the Cr_2C seed, the N layers occupy either H_C or empty Hollow (H) sites. Notice in passing by that such Janus structures are not observed on M_2N seeds, succinctly suggesting that such different surface terminations come from having alternate C and N layers across the MXene structure.

Having defined and optimized the structure of M_2XN_2 models, two neighboring N vacancies were generated on one of the two surfaces—or the different surface endings in the case of Janus models—and the resulting model was used to investigate the N_2 adsorption energy for $\theta_N = 7/9$ ML, explored on the N-free surface patch. The calculated adsorption energies are listed in Table S4 of the SI, and reveal that, in general terms, such surface N-free patches maintain a chemical affinity towards N_2 , with negative $E_{ads}^{N_2}$ values going from -0.43 (Zr_2N) to -2.05 eV (Ta_2N). However, on this fourth criterion, one starts finding certain cases where a full N-coverage is not likely to be met. For instance, Mo_2C shows an adverse $E_{ads}^{N_2}$ of 0.97 eV. Further than that, group VI N-based MXenes, Cr_2N , Mo_2N , and W_2N , as well as W_2C and V_2C , still feature negative N_2 adsorption energies, yet weaker than -0.2 eV, and so are catalogued as dubious cases in Figure 1.

Two more surprising trends emerge within this criterion; first, at variance with the $\theta_N = 0$ ML results shown in Table S2 of the SI, the N-based group V MXenes (V_2N , Nb_2N , Ta_2N) display sensibly stronger $E_{ads}^{N_2}$ values, fringed between -0.87 (V_2N) and -2.05 eV (Ta_2N), when compared to C-based seeds, going from -0.2 (V_2C) to -1.20 eV (Ta_2C). The second curious feature is that Cr_2C , displaying a Janus structure, shows a remarkably distinct N_2 affinity depending on whether the N adatoms occupy H_C or H sites, going from a markedly exothermic adsorption of -1.65 eV on the H_C ending, to a notably endothermic adsorption of 0.5 eV on the H ending. This distinct chemical activity could imply that a $\theta_N = 1$ ML can be reached on the H_C side, while only a partial θ_N could be achieved on the other H surface ending.

When it comes to the N_2 dissociation energy barrier at a near $\theta_N = 1$ ML situation, one readily observes in Figure 1 that this is indeed the most stringent explored criterion, not met in ten out of 18 MXenes. The values, listed in Table S4 of the SI, reveal cases with high $E_b^{N_2}$ values, such as group IV M_2N seeds, that is, Ti_2N , Zr_2N , and Hf_2N , with barriers

surpassing 5.4 eV. These prohibitive barriers are the result of moderate $E_{\text{ads}}^{\text{N}_2}$ values, not exceeding -0.53 eV, and so, basically depicting a physisorption state in which the N_2 molecular bond is neither compromised nor activated towards its breakage. This is to be put together with large $\Delta E_{\text{dis}}^{\text{N}_2}$ values above 4.1 eV, see discussion below; implying that the reaction step is thermodynamically quite endothermic and, concomitantly, requires surpassing large energy barriers. The rest of the estimated $E_{\text{b}}^{\text{N}_2}$ are more moderate, framing very likely situations, such as the barrier of solely 0.24 eV of Nb_2N , to sensibly large values such as the 2.81 eV for the H_C -terminated surface on Cr_2C . In any case, the $E_{\text{b}}^{\text{N}_2}$ values have to be compared to the desorption energy values and, in this regard, only Zr_2C , Nb_2N , Ta_2C , and the H_C surface of Hf_2C , yet closely followed by dubious cases of V_2N , Ta_2N , Mo_2C , H_M surface termination on Hf_2C , and H termination of Cr_2C , can be considered viable.

The exothermic $\Delta E_{\text{dis}}^{\text{N}_2}$ criterion is, in comparison, achieved in a larger number of cases. Apart from the just mentioned group IV M_2N cases, only Cr_2N (1.32 eV) and W_2C (0.68 eV) feature clearly endothermic situations, and basically isoenergetic situations are found for H_C surface termination of Cr_2C , plus Mo_2N and W_2N . Other than these cases, the N_2 dissociation into N adatoms at a high θ_{N} coverage is clearly exothermic, ranging from -0.60 (Ta_2N) to -3.36 eV (Ta_2C). Notice that, even though this last dissociative step may be endothermic, the analysis of the M_2XN_2 formation energies is constantly exothermic, see Figure 1, and E_{form} values displayed in Table S4 of the SI, going from -1.46 (Cr_2CN_2) to -4.28 eV (Ta_2CN_2). Thus, such M_2XN_2 MXenes are thermodynamically favorable, although, in light of the results, some reaction steps may be thermodynamically uphill, and in some cases, kinetically hindered; especially when reaching nearly full θ_{N} coverage situations. Notice, however, that even whenever N_2 adsorption and/or dissociation is not favorable at such coverage limit, one may envision N -terminated domains, which may allow for *a posteriori* deposition of metal atoms.

Taking again the Ta_2C seed example shown in Figure 2, the reaction profile for the N_2 adsorption and dissociation on the nearly fully N -covered model is shown in Figure 5, here revealing an $E_{\text{ads}}^{\text{N}_2}$ of -1.20 eV, still larger than the N_2 dissociation energy barrier, $E_{\text{b}}^{\text{N}_2}$, of 0.73 eV, leading to the formation of the Ta_2CN_2 (0001) surface, with a reaction energy, $\Delta E_{\text{dis}}^{\text{N}_2}$, of -3.36 eV, revealing how favorable the formation of Ta_2CN_2 is, with an E_{form} of -4.28 eV per structural unit. The elementary reaction rates are shown in Figure 6,

alongside with the built kinetic phase diagram, revealing a somewhat smaller region for N_2 adsorption compared to the pristine case shown in Figure 3. Furthermore, for low temperatures, r_{dis} is larger than r_{des} , but there is a limit temperature, T_1 , of 663 K, from which the adsorbed N_2^* would more likely desorb than dissociate and, therefore, a preference towards having N_2^* is forecasted. Still, the N_2 dissociation capability is still featured, revealing that, at $p_{N_2} = 1$ bar, one could complete the N^* full coverage at working temperatures below *ca.* 594 K.

Having analyzed the possibility of acquiring N-terminated M_2XN_2 MXenes, the next step is to investigate whether they can finally become metal-covered. To this end, we firstly inspected the adsorption of a single M' atom on M_2XN_2 MXenes, where M' is one of the MXenes M constituents; this is, from group IV (Ti, Zr, Hf), V (V, Nb, Ta) or VI (Cr, Mo, W). The M' adatom was adsorbed respecting the regular M_2XN_2 stacking; H_X sites for regular ABC stacking and H_M for regular ABA stacking. In the case of Janus endings, different hollow sites were evaluated, although there is a preference trend for M' being adsorbed on hollows with no underlying atoms in the two first subsurface layers, which are H and H_C sites for H_C and H_M sides of Janus Ti_2CN_2 , Zr_2CN_2 , and Hf_2CN_2 , and H_C and H sites for H and H_C N-endings of Cr_2CN_2 . A complete list of sites and the corresponding $E_{\text{ads}}^{M'}$ values is compiled in Table S5 of the SI.

The definition of $E_{\text{ads}}^{M'}$ already implies that for negative values there is a preference for M' to adsorb on the M_2XN_2 model rather than staying fully coordinated in the M' bulk environment, and therefore, underscoring a thermodynamic preference for having such metals as isolated adatoms. This hints towards the possible use of M_2XN_2 as substrates for such M' surface single atoms (SAs), employable as specially engineered atomic centers,⁵³ as seen in the past for pristine MXenes and other 2D carbon-based materials,⁴⁵⁻⁴⁷ although the analysis of SAs on these MXenes is not the goal of the present paper. Therefore, we just mention that, in the explored cases, it seems clear that when going along the d series, the possibility of having isolated M' adatoms becomes less favorable, see Figure 4, in which group VI M' (Cr, Mo, W) start to be unfavorable towards M' adatom isolation. This is mostly due to the higher cohesive energies displayed by transition metals along the d series up to the d^5 configurations, as a result of filling the bonding states of the d -band.^{46,54}

However, the above is no rule-of-thumb, and the possibility to find M' isolated also depends on the considered M_2XN_2 substrate, with several cases being found where M'

single adatom adsorption is favorable. In particular, this happens for Ti_2NN_2 , Zr_2NN_2 , and Hf_2NN_2 group IV M_2N MXenes, yet closely followed by V_2CN_2 . Also, the adsorption strength ranges from weak, *e.g.* $E_{\text{ads}}^{\text{M}'}$ is -0.21 eV for Zr on the H_M side of Hf_2CN_2 , to rather strong, with a value of -8.84 eV for Hf adatoms on W_2CN_2 . Indeed, such highly exothermic values contrast with the adatom preference on pristine M_2C (0001) surfaces, of -0.95 eV at most for Sc adatoms on Cr_2C , using the same models and computational setup as the ones employed here.⁴⁷ As found on previous systematic studies on the transition metal adatoms stability on extended graphene and graphyne substrates,^{46,54} M' adsorption strength enhancement may well be related to the inherent substrate instability. This would explain why the M' adsorption is weak on pristine M_2X MXenes, that, even if metastable, are experimentally reachable, whereas M' adatoms can attach more strongly on N-terminated M_2X models, that, even if thermodynamically and kinetically driven, can be less stable, as experimentally only MXenes with $-\text{NH T}_x$ have been isolated and characterized.²² Thus, such M_2XN_2 models have to be considered as intermediate cases, as would likely adsorb hydrogen, metal atoms, or other species so as to coat them, bestowing stability in this process.

In the search for $\text{M}_2'\text{M}_2\text{XN}_2$ we next analyze the $E_{\text{ads}}^{\text{M}'}$ criterion for an almost full M' surface coverage of $\frac{8}{9}$ ML, thus, featuring a single M' vacancy on which the M' is adsorbed, in order to scrutinize whether the formation of a monolayer is preferred over M' clustering, *i.e.* favoring an epitaxial growth instead of the island/nanoparticle formation. The calculated values are compiled in Table S6 of the SI, and the results visually summarized in Figure 7. As expected, both the exothermicity and the number of favorable cases decrease, given the lateral repulsions and the metal adlayer inherent tension to be commensurate to the M_2XN_2 seed. In general, and as seen in Figure 7, M' adlayers are disfavored not only for group VI (Cr, Mo, W), but also in several group V (V, Nb, Ta) cases, and even for certain group IV (Ti, Zr, Hf) situations. In any case, it is worth mentioning that, for all the M_2X seeds and M_2XN_2 models, there is at least one M' metal from which an adlayer formation would be thermodynamically driven, and that is why the low and high coverage $E_{\text{ads}}^{\text{M}'}$ criteria are generally met in Figure 1. The only exception to this is the H_C side of Ti_2C , where the single adatom adsorption is dubious for Ti, Zr, and Hf, see Figure 7.

Finally, even if the first and last adatom adsorptions are thermodynamically possible during the formation of an M' adlayer, the formation energies of the resulting surface,

E_{form} , are analyzed in the last decalogue criterion. The computed values are displayed in Table S7 of the SI, and graphically shown in Figure 8. From this Figure, a clear pattern arises; the formation energies become more positive, and concomitantly thermodynamically less favored, when going along the M' d series, *i.e.* when moving from groups IV to VI, to the point of being generally not favorable for any group VI M', except for the case of $\text{Mo}_2\text{Ti}_2\text{NN}_2$, with an E_{form} of -0.35 eV. On the contrary, group IV M' adlayers seem to be thermodynamically suited regardless of the M_2X seed, with values ranging from mild, -0.49 eV for Zr on W_2CN_2 , to highly exothermic, -4.43 eV for Ti on Ti_2NN_2 , *i.e.* the epitaxial synthesis of Ti_4N_3 , encouragingly, coinciding with the first example of a stable two-dimensional transition metal nitride, which was attained experimentally through the selective etching of Al from a MAX phase precursor.⁵⁵ This is again partly due to the above-mentioned larger cohesive energy encountered for transition metals when increasing the number of d electrons, at least up to d^5 configurations, filling all the bonding states. Notice as well that, according to the present computational framework, the epitaxial synthesis of M_4N_3 MXenes should be feasible. This is an important issue since, despite having been forecasted to be more stable than M_4C_3 , they have not yet been successfully synthesized, at variance with their C-based MXene counterparts.^{2,56} Notice, aside, that once an $\text{M}'_2\text{M}_2\text{XN}_2$ MXene is obtained, it can be used as a further seed to obtain MXenes with larger n , and that, furthermore, given the similar chemical activity of M_{n+1}X_n MXenes, seeds with $n = 2, 3$ could well be used for the epitaxial growth, as a way of obtaining $n > 3$ MXenes.

Retaking the Ta_2C (0001) seed prototypical case, Figures 2 and 5 showed the viability of having a fully N-covered situation, accomplishing both thermodynamic and kinetic thresholds. Furthermore, the formation energy of Ta_2CN_2 is -4.28 eV, thus strongly suggesting the stability of this N-terminated MXene. The adsorption of the first Ti adatom on Ta_2CN_2 features an $E_{\text{ads}}^{\text{M}'}$ of -1.32 eV with respect to Ti bulk, and a similar value of -1.29 eV is found for the completion of the $\text{Ti}_2\text{Ta}_2\text{CN}_2$ MXene, whose formation energy with respect to Ta_2CN_2 and bulk Ti is -1.98 eV. This is just one example out of the many studied showing how the decalogue of criteria for MXene epitaxial growth is accomplished, meeting all the required stability and kinetic thresholds. Actually, one could foresee, *e.g.* the use of the as-synthesized $\text{Ti}_2\text{Ta}_2\text{CN}_2$ MXene as a seed to grow thicker MXenes, even mixing different metallic compositions at different materials strata. Indeed, as a proof of concept, the N_2 adsorption energy on $\text{Ti}_2\text{Ta}_2\text{CN}_2$ was computed to

be -3.19 eV, nicely lying in between the values for Ta₂C (seed) and Ti₂N (growth), of -2.35 and -3.45 eV, respectively, succinctly unfolding that the tailored epitaxial growth on selected MXene seeds can be used as a way of fine-tuning the MXene surface chemical activity, and enlarges the *o*-MXenes family offering a way to control its layer composition.

One should bear in mind, though, that even when all the decalogue criteria are met, other aspects may determine whether a certain MXene or *o*-MXene could be epitaxially grown as foreshown. For instance, the MXene M₂X seed, the intermediate M₂XN₂, and the final resulting M'₂M₂XN₂ MXene should be dynamically stable. Actually, many pristine and functionalized MXenes have been shown to be dynamically stable in the literature.⁵⁷⁻⁶¹ In the present case, we explored the dynamic stability on the exemplary case of Ta₂C seed, the Ta₂CN₂ intermediate, and the final Ti₂Ta₂CN₂ MXene by appropriate phonon calculations. The results are summarized in Figure 10, where acoustic and optical vibrational modes dispersions in the **k**-space —along main $\Gamma \rightarrow \mathbf{M} \rightarrow \mathbf{K} \rightarrow \Gamma$ **k**-paths with a convergence criterion of 10⁻⁸ eV— have been gained through Density Functional Perturbation Theory (*DFPT*) as implemented in the PHONOPY code.⁶² The dynamical stability of such cases is clear from the absence of imaginary frequencies in the selected **k**-path. Even if proven in such an exemplary case, such assessment would be useful for other systems, although the previous studies and the present evaluation seem to guarantee that there will be a number of situations where the epitaxial growth would be feasible.

Another aspect to regard beyond the dynamic stability is whether the explored M'₂M₂XN₂ MXenes would actually remain layered as designed, or whether in-plane alloying of M' and M could be expected, as observed experimentally in the so-called *i*-MXenes.^{57,63} To at least address this point on the exemplary case of Ti₂Ta₂CN₂, different arrangements were evaluated assuming the same overall stoichiometry, but having equal parts of Ti and Ta on the metal layers. The results, summarized in Figure S3 of the SI, reveal that any *i*-MXene alloy configuration is higher in energy, with differences in energy, ΔE , ranging from 0.01 to 0.15 eV, referred to a *p*(2×2) unit cell of Ti₂Ta₂CN₂. Given that some cases are basically isoenergetic, the interchange of surface Ti with subsurface Ta atom was further investigated, but the sequential interchange of Ti↔N↔Ta leads to either situations very high in energy, above 8 eV, or to jeopardized MXene structures. Thus, the only viable way of having metal disorder is through the presence of vacancies. Indeed, the surface Ti diffusing to a subsurface Ta vacancy is

thermodynamically favorable by -1.98 eV, but still surmounting a costly energy barrier of 2.26 eV. Only when having vicinal Ta and N vacancies, the Ti diffusion is energetically favorable by -2.28 eV, with a moderate energy barrier of 0.60 eV. However, it must be borne in mind that having such vicinal vacancies are energetically costly, with a formation energy calculated to be of 5.28 eV with respect Ta bulk and N₂ gas. Even if spontaneous alloying in Ti₂Ta₂CN₂ seems unlikely, the situation may change for other mixtures, a point to be regarded in future studies. However, the metal alloying on epitaxially grown MXenes is something worthy to be analyzed, and that even can be prompted, by depositing given quantities of a couple of metals, a point that widens the possibilities of manufacturing different MXenes by epitaxial growth.

4. Conclusions

In summary, we provided here an atomistic radiography of the plausible epitaxial growth of MXenes by depositing alternating layers of N and early transition metal atoms on a set of 18 carbide and nitride M₂X MXene seeds, considering the energetically most stable stacking conformation, and scrutinizing a decalogue of thermodynamic and kinetic energy criteria of different growth steps by first-principles calculations.

The results show that, while pristine M₂X (0001) surfaces systematically easily adsorb and dissociate N₂, the formation of fully N-covered M₂XN₂ models may be kinetically hindered depending on the employed M₂X seed, being thus the most restrictive criterion and reaction step, even though the formation energy of M₂XN₂ models is thermodynamically advantageous. In the case of group IV Ti₂C, Zr₂C, and Hf₂C, as well as of Cr₂C, different surface N-endings are found, rendering these M₂XN₂ MXenes effectively Janus structures.

The formation of early transition metal additional adlayers leading to new M'₂M₂XN₂ MXenes is, in general, thermodynamically driven for all the M₂XN₂ models, although there are exceptions to this trend. In any case, a route map in the epitaxial growth of MXenes by alternating N and metal adlayers is provided, based on which further casts can be made. Furthermore, the presented epitaxial growth is introduced as a way of achieving the M₄N₃ synthesis, obtaining wider MXenes going beyond seven layers, and/or tuning the MXene formulation, generating *o*-MXenes at will. The present work is expected to trigger new experimental work aiming at obtaining new MXenes by exploiting the epitaxial growth as here analyzed and proposed.

Associated Content

Supporting Information

The following Supporting Information is available free of charge on the ACS Publications website at DOI:

Difference in energies between non-magnetic, ferromagnetic, and antiferromagnetic solutions. N₂ adsorption energies, dissociation energy barriers, and dissociation energy changes on pristine and nearly fully N-covered M₂X (0001) MXene models. M₂XN₂ formation energies and differences in energy between ABC and ABA stacking conformations for M₂X and M₂XN₂ models. M' adsorption energies on M₂XN₂ models and nearly M' fully covered M₂XN₂ models. M'₂M₂XN₂ formation energies. Difference in energies for diverse alloys of Ti₂Ta₂CN₂ MXene model.

Acknowledgements

The work carried out at the *Universitat de Barcelona* has been supported by the Spanish MCIN/AEI/10.13039/501100011033 RTI2018-095460-B-I00 (funded partially from FEDER *Una manera de hacer Europa*) and *María de Maeztu* MDM-2017-0767 project and the work carried out at CICECO-Aveiro Institute of Materials has been financed through projects UIDB/50011/2020, UIDP/50011/2020 and LA/P/0006/2020, financed by national funds through the *Fundação para a Ciência e a Tecnologia* (FCT/MCTES) and co-financed by FEDER under the PT2020 Partnership Agreement. A.M.-G. thanks the support by the PID2020-115293RJ-I00 project funded by MCIN/AEI/10.13039/501100011033, and J.D.G. thanks project SILVIA with references CENTRO-01-0145-FEDER-31002 and PTDC/QUI-QFI/31002/2017. We are also thankful to FCT I.P. for the computational resources granted in the framework of project EPICNITRO (Ref. CPCA/A2/6817/2020) by the FCT/CPCA/2020/01 Call for Advanced Computing Projects.

Figure 1. Summary of accomplishment of the ten (*i-x*) decalogue criteria for epitaxial growth alternating N and M' adlayers over a M₂X central MXene seed. The upper tags represent the followed criteria at certain given coverage conditions. Right tags denote different surface endings for some M₂XN₂ models. Light green (red) color implies meeting (or not) the sought criterion, while light yellow color implies dubious cases within the DFT ± 0.2 eV accuracy range. H_C and H_M denote hollow sites where the adatoms are vertically aligned with a carbon or metal, respectively.

	$\theta_N = 0$ ML			$\theta_N \sim 1$ ML							
	$N_2^{ads} < 0$	$N_2^{ads} < -E_{ads}$	$\Delta E_{dis}^{N_2} < 0$	$N_2^{ads} < 0$	$N_2^{ads} < -E_{ads}$	$\Delta E_{dis}^{N_2} < 0$	$E_{form}^{M_2XN_2} < 0$	$E_{ads}^{M'} < E_{coh}^{M'} \theta_{M'} = 0$ ML	$E_{ads}^{M'} < E_{coh}^{M'} \theta_{M'} = 1$ ML	$E_{form}^{M'_2M_2XN_2} < 0$	
Ti ₂ C	Light Green	Light Green	Light Green	Light Green	Light Green	Light Green	Light Green	Light Green	Light Green	Light Green	H _C
Ti ₂ N	Light Green	Light Green	Light Green	Light Green	Light Green	Light Green	Light Green	Light Green	Light Green	Light Green	H _M
Zr ₂ C	Light Green	Light Green	Light Green	Light Green	Light Green	Light Green	Light Green	Light Green	Light Green	Light Green	H _C
Zr ₂ N	Light Green	Light Green	Light Green	Light Green	Light Green	Light Green	Light Green	Light Green	Light Green	Light Green	H _M
Hf ₂ C	Light Green	Light Green	Light Green	Light Green	Light Green	Light Green	Light Green	Light Green	Light Green	Light Green	H _C
Hf ₂ N	Light Green	Light Green	Light Green	Light Green	Light Green	Light Green	Light Green	Light Green	Light Green	Light Green	H _M
V ₂ C	Light Green	Light Green	Light Green	Light Green	Light Green	Light Green	Light Green	Light Green	Light Green	Light Green	
V ₂ N	Light Green	Light Green	Light Green	Light Green	Light Green	Light Green	Light Green	Light Green	Light Green	Light Green	
Nb ₂ C	Light Green	Light Green	Light Green	Light Green	Light Green	Light Green	Light Green	Light Green	Light Green	Light Green	
Nb ₂ N	Light Green	Light Green	Light Green	Light Green	Light Green	Light Green	Light Green	Light Green	Light Green	Light Green	
Ta ₂ C	Light Green	Light Green	Light Green	Light Green	Light Green	Light Green	Light Green	Light Green	Light Green	Light Green	
Ta ₂ N	Light Green	Light Green	Light Green	Light Green	Light Green	Light Green	Light Green	Light Green	Light Green	Light Green	
Cr ₂ C	Light Green	Light Green	Light Green	Light Green	Light Green	Light Green	Light Green	Light Green	Light Green	Light Green	H _C
Cr ₂ N	Light Green	Light Green	Light Green	Light Green	Light Green	Light Green	Light Green	Light Green	Light Green	Light Green	H
Mo ₂ C	Light Green	Light Green	Light Green	Light Green	Light Green	Light Green	Light Green	Light Green	Light Green	Light Green	
Mo ₂ N	Light Green	Light Green	Light Green	Light Green	Light Green	Light Green	Light Green	Light Green	Light Green	Light Green	
W ₂ C	Light Green	Light Green	Light Green	Light Green	Light Green	Light Green	Light Green	Light Green	Light Green	Light Green	
W ₂ N	Light Green	Light Green	Light Green	Light Green	Light Green	Light Green	Light Green	Light Green	Light Green	Light Green	
	<i>i</i>	<i>ii</i>	<i>iii</i>	<i>iv</i>	<i>v</i>	<i>vi</i>	<i>vii</i>	<i>viii</i>	<i>ix</i>	<i>x</i>	

Figure 2. Reaction energy profile for N₂ adsorption on the pristine Ta₂C (0001) surface model, and its subsequent dissociation into 2 N adatoms, overcoming the reaction step TS. The atomic models display the different stages of the process, with Ta, C, and N atoms represented by light green, light brown, and blue spheres, respectively.

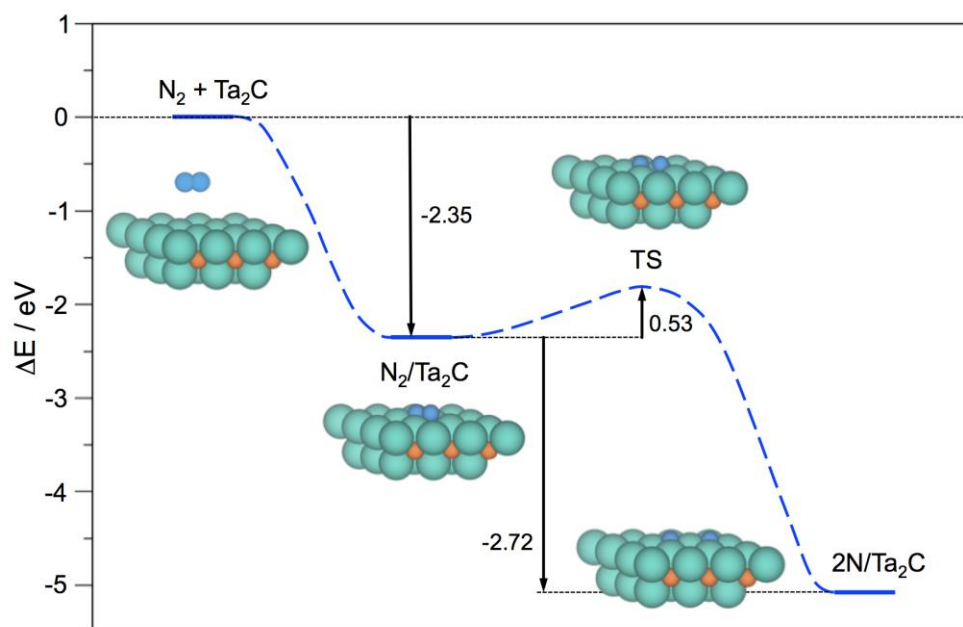


Figure 3. Top panel: Elementary reaction rates on Ta₂C (0001) surface for the N₂ adsorption at 0.1 bar as a function of temperature, T . The r_{ads} and r_{des} quantities stand for adsorption and desorption rates, respectively, whereas r_{dis} and r_{rec} correspond to the N₂ dissociation and 2N recombination rates, respectively. Bottom panel: Kinetic phase diagram for N₂ adsorption and dissociation as a function of N₂ partial pressure, p_{N_2} , and T . Dark blue colored areas reveal regions of preference towards N* moiety.

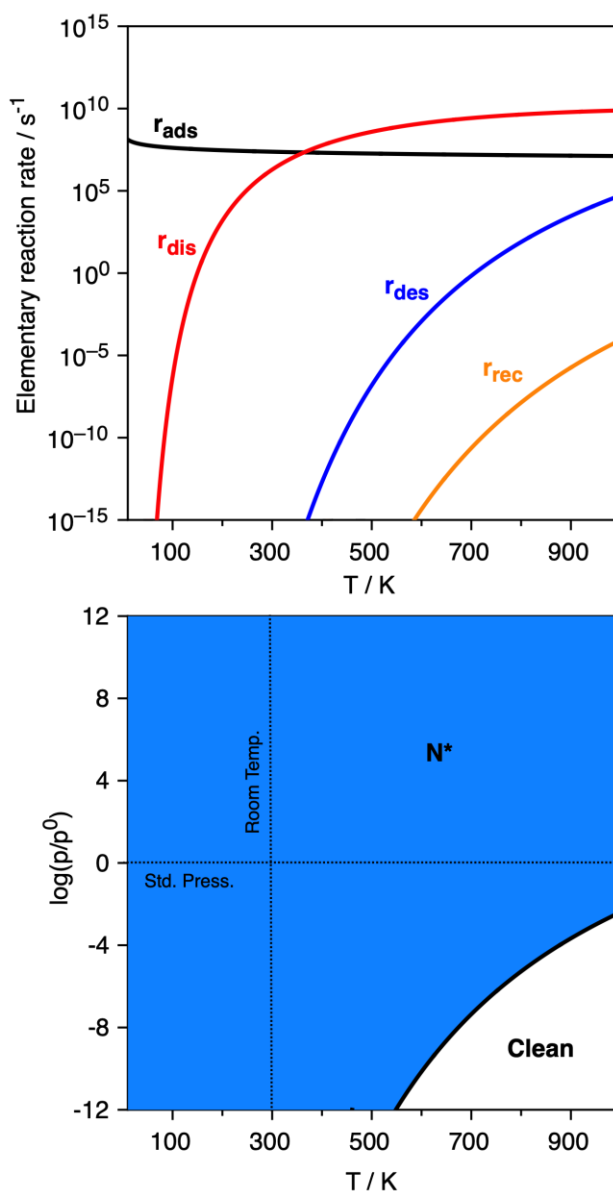


Figure 4. Plots of ΔE_{stack} as a function of the M element for X = C (black) or N (blue) M_2X seed compositions, either for pristine (top panel)³² or N-terminated (bottom panel) models. The red dashed line denotes equal energetic stability between ABC and ABA stackings, with negative values indicating preference for the latter.

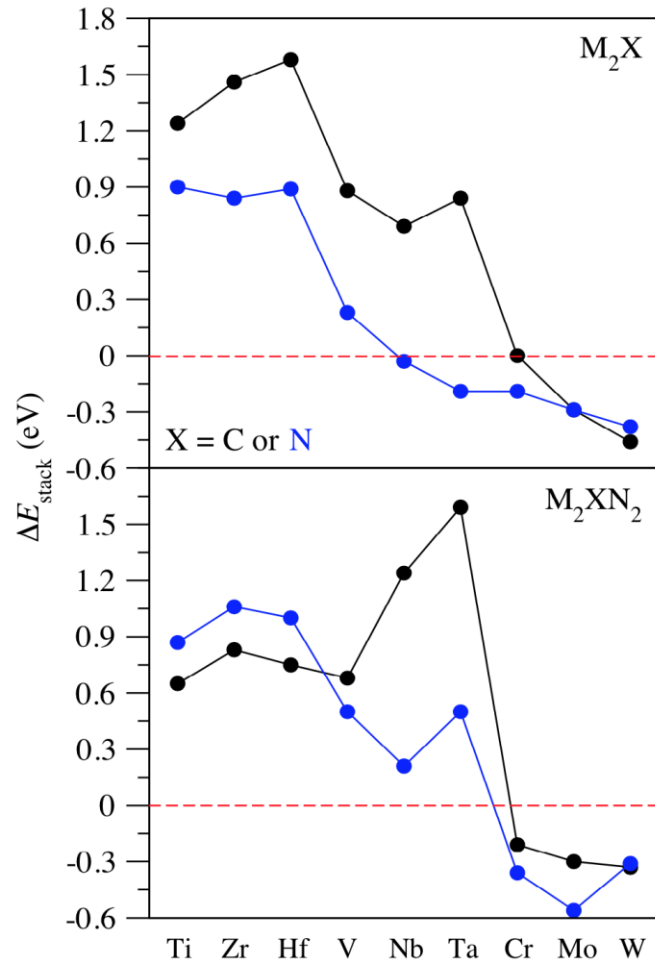


Figure 5. Reaction energy profile for N₂ adsorption on the nearly full N-covered Ta₂CN_x (0001) surface model, and its subsequent dissociation into 2 N adatoms, overcoming the reaction step TS, to get finally the Ta₂CN₂ structure. The atomic models represent the different stages of the process. Color coding as in Figure 2.

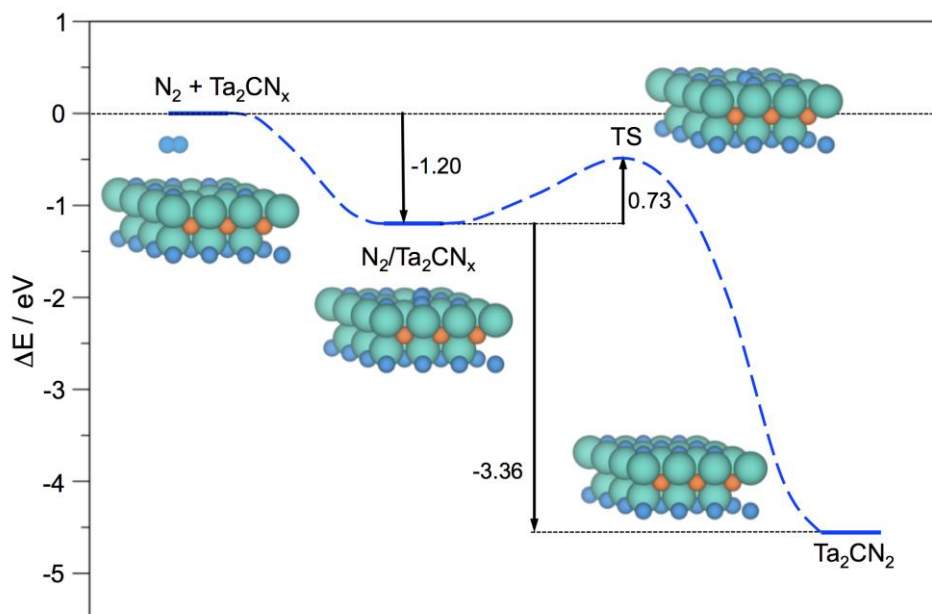


Figure 6. Top panel: Elementary reaction rates on the nearly fully N-covered Ta₂C (0001) surface for the N₂ adsorption at 0.1 bar as a function of temperature, T . The quantities r_{ads} , r_{des} , r_{dis} and r_{rec} are defined as in Figure 3. Notice that at the T_1 temperature of 663 K, $r_{\text{dis}} = r_{\text{des}}$, and from this temperature upwards, desorption rate is larger than N₂ dissociation rate. Bottom panel: Kinetic phase diagram for N₂ adsorption and dissociation as a function of N₂ partial pressure, p_{N_2} , and T . Dark and light blue colored areas reveal regions of preference towards N* and N₂* moieties, respectively.

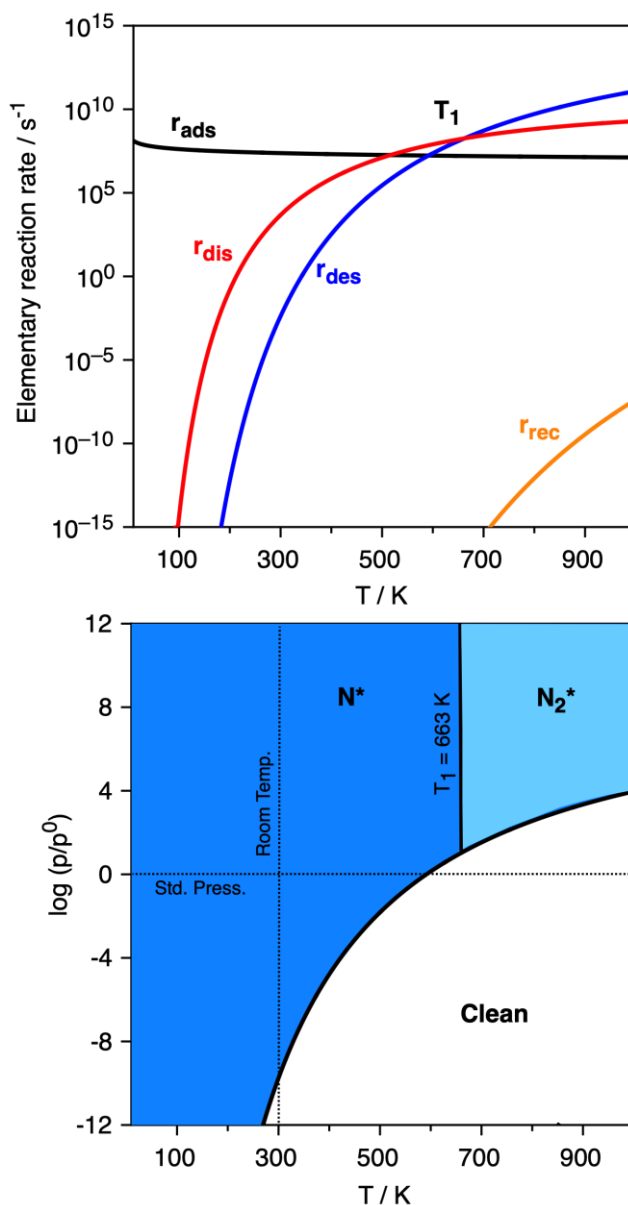


Figure 7. Degree of accomplishment of criteria *viii* and *ix*, implying M' adsorption energies on pristine (left panel) or on nearly M' fully covered (right panel) M_2XN_2 MXene models. Light green (red) color implies meeting (or not) the sought criterion, while light yellow color implies dubious cases within the DFT ± 0.2 eV accuracy range. H_C and H_M denote hollow sites where the adatoms are vertically aligned with a carbon or metal, respectively.

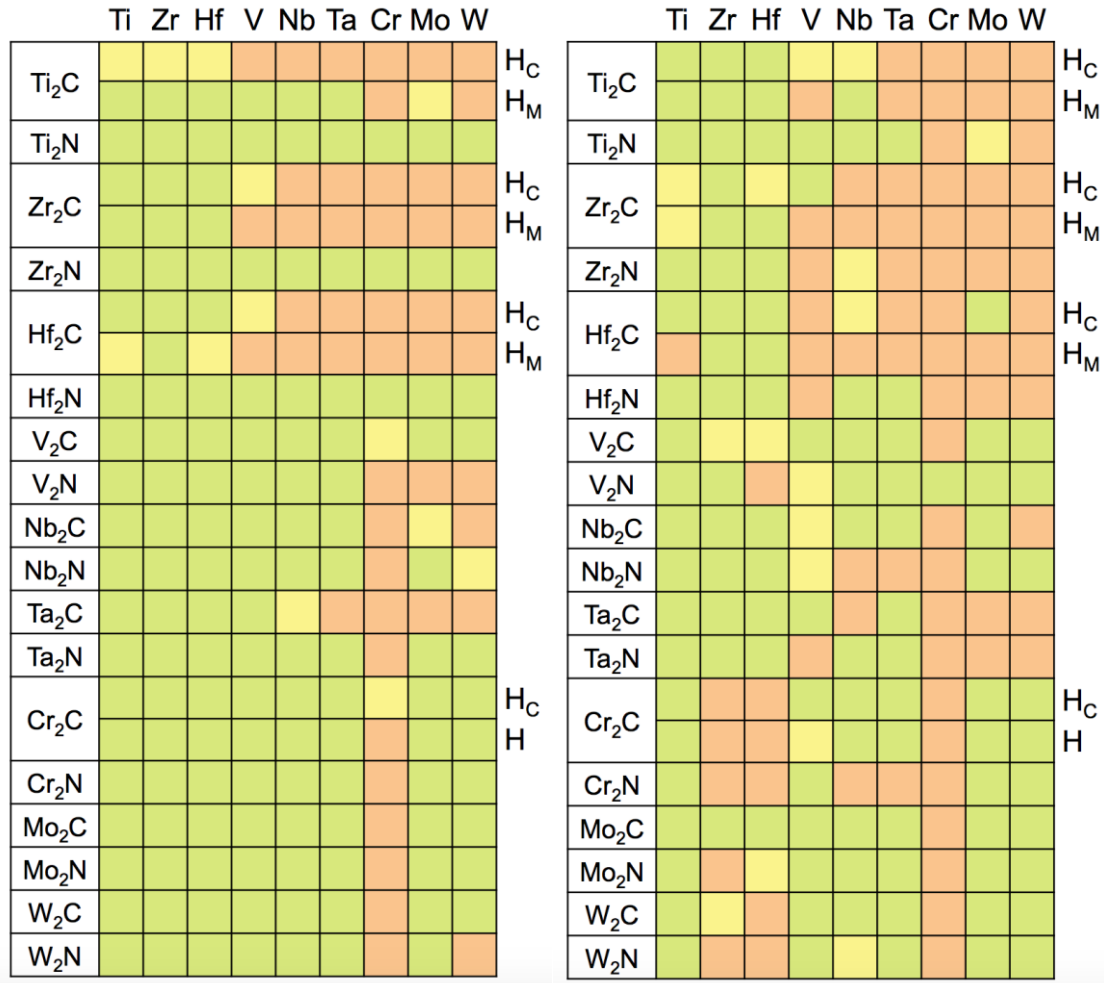


Figure 8. Degree of accomplishment of criteria x , *i.e.*, $M'_2M_2XN_2$ MXenes formation energies. Light green (red) color implies meeting (or not) the sought criterion, while light yellow color implies dubious cases within the DFT ± 0.2 eV accuracy.

	Ti	Zr	Hf	V	Nb	Ta	Cr	Mo	W
Ti ₂ C	Light Green	Light Green	Light Green	Light Green	Light Green	Light Orange	Light Orange	Light Orange	Light Orange
Ti ₂ N	Light Green	Light Green	Light Green	Light Green	Light Green	Light Green	Light Orange	Light Green	Light Orange
Zr ₂ C	Light Green	Light Green	Light Green	Light Orange	Light Orange	Light Orange	Light Orange	Light Orange	Light Orange
Zr ₂ N	Light Green	Light Green	Light Green	Light Green	Light Green	Light Green	Light Orange	Light Orange	Light Orange
Hf ₂ C	Light Green	Light Green	Light Green	Light Orange	Light Orange	Light Orange	Light Orange	Light Orange	Light Orange
Hf ₂ N	Light Green	Light Green	Light Green	Light Green	Light Green	Light Green	Light Orange	Light Orange	Light Orange
V ₂ C	Light Green	Light Green	Light Green	Light Green	Light Green	Light Green	Light Orange	Light Orange	Light Orange
V ₂ N	Light Green	Light Green	Light Green	Light Green	Light Green	Light Green	Light Orange	Light Orange	Light Orange
Nb ₂ C	Light Green	Light Green	Light Green	Light Green	Light Green	Light Yellow	Light Orange	Light Orange	Light Orange
Nb ₂ N	Light Green	Light Green	Light Green	Light Green	Light Yellow	Light Orange	Light Orange	Light Orange	Light Orange
Ta ₂ C	Light Green	Light Green	Light Green	Light Green	Light Orange	Light Orange	Light Orange	Light Orange	Light Orange
Ta ₂ N	Light Green	Light Green	Light Green	Light Yellow	Light Yellow	Light Orange	Light Orange	Light Orange	Light Orange
Cr ₂ C	Light Green	Light Green	Light Green	Light Green	Light Green	Light Green	Light Orange	Light Orange	Light Orange
Cr ₂ N	Light Green	Light Green	Light Green	Light Green	Light Green	Light Green	Light Orange	Light Yellow	Light Orange
Mo ₂ C	Light Green	Light Green	Light Green	Light Green	Light Green	Light Green	Light Orange	Light Orange	Light Orange
Mo ₂ N	Light Green	Light Green	Light Green	Light Green	Light Green	Light Green	Light Orange	Light Orange	Light Orange
W ₂ C	Light Green	Light Green	Light Green	Light Green	Light Green	Light Green	Light Orange	Light Orange	Light Orange
W ₂ N	Light Green	Light Green	Light Green	Light Green	Light Yellow	Light Orange	Light Orange	Light Orange	Light Orange

Figure 9. Steps of formation of Ta_2CN_2 and $\text{Ti}_2\text{Ta}_2\text{CN}_2$ models departing from Ta_2C seed, alongside with the formation energies for each step. Ti atoms are shown as grey spheres, while the rest of the color coding is as in Figure 2.

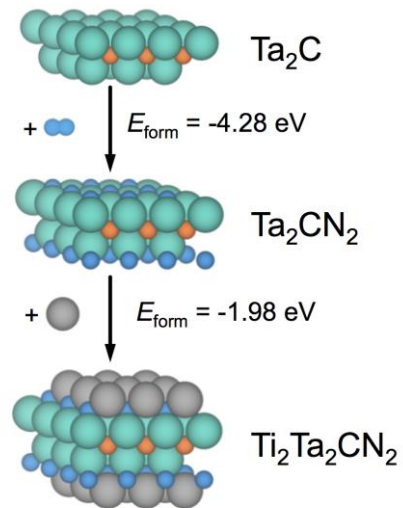
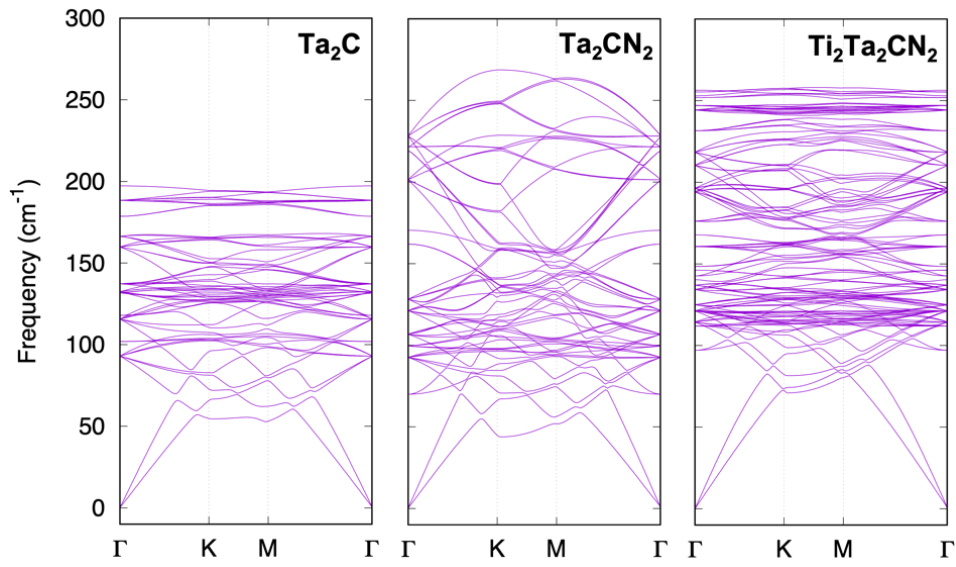


Figure 10. Phonon dispersion curves for Ta_2C , Ta_2CN_2 , and $\text{Ti}_2\text{Ta}_2\text{CN}_2$ MXenes, along the main $\Gamma \rightarrow \text{M} \rightarrow \text{K} \rightarrow \Gamma$ \mathbf{k} -path in the Brillouin zone of the reciprocal space.



References

- (1) Naguib, M.; Kurtoglu, M.; Presser, V.; Lu, J.; Niu, J.; Heon, M.; Hultman, L.; Gogotsi, Y.; Barsoum, M. W. Two-Dimensional Nanocrystals Produced by Exfoliation of Ti_3AlC_2 . *Adv. Mater.* **2011**, *23*, 4248–4253.
- (2) Gogotsi, Y.; Anasori, B. The Rise of MXenes. *ACS Nano* **2019**, *13*, 8491–8494.
- (3) Tang, X.; Guo, X.; Wu, W.; Wang, G. 2D Metal Carbides and Nitrides (MXenes) as High-Performance Electrode Materials for Lithium-Based Batteries. *Adv. Energy Mater.* **2018**, *8*, 1801897.
- (4) Han, M.; Shuck, C. E.; Rakhmanov, R.; Parchment, D.; Anasori, B.; Koo, C. M.; Friedman, G.; Gogotsi, Y. Beyond $\text{Ti}_3\text{C}_2\text{T}_x$: MXenes for Electromagnetic Interference Shielding. *ACS Nano* **2020**, *14*, 5008–5016.
- (5) Morales-García, Á.; Fernández-Fernández, A.; Viñes, F.; Illas, F. CO_2 Abatement Using Two-Dimensional MXenes Carbides. *J. Mater. Chem. A* **2018**, *6*, 3381–3385.
- (6) Morales-Salvador, R.; Morales-García, Á.; Viñes, F.; Illas, F. Two-Dimensional Nitrides as Highly Potential Candidates for CO_2 Capture and Activation. *Phys. Chem. Chem. Phys.* **2018**, *20*, 17117–17124.
- (7) Persson, I.; Halim, J.; Lind, H.; Hansen, T. W.; Wagner, J. B.; Näslund, L.-Å.; Darakchieva, V.; Palisaitis, J.; Rosen, J.; Persson, P. O. Å. 2D Transition Metal Carbides (MXenes) for Carbon Capture. *Adv. Mater.* **2019**, *31*, 1805472.
- (8) Gouveia, J. D.; Novell-Leruth, G.; Reis, P.; Viñes, F.; Illas, F.; Gomes, J. R. B. First-Principles Calculations of the Adsorption Behavior of Amino Acids on a Titanium Carbide MXene. *ACS Appl. Bio Mater.* **2020**, *3*, 5913-5921.
- (9) Gouveia, J. D.; Novell-Leruth, G. ; Viñes, F.; Illas, F.; Gomes, J. R. B. The Ti_2CO_2 MXene as a Nucleobase 2D Sensor: a First-Principles Study. *Appl. Surf. Sci.* **2021**, *544*, 148946.
- (10) Shevchuk, K.; Sarycheva, A.; Gogotsi, Y. Evaluation of Two-Dimensional Transition-Metal Carbides and Carbonitrides (MXenes) for SERS Substrates. *MRS Bull.* **2022**, in press, <https://doi.org/10.1557/s43577-022-00276-8>.
- (11) Li, Y.; Peng, Z.; Holl, N. J.; Hassan, R.; Pappas, J. M.; Wei, C.; Izadi, O. H.; Wang, Y.; Dong, X.; Wang, C.; Huang, Y.-W.; Kim, D. H.; Wu, C. MXene–

-
- Graphene Field-Effect Transistor Sensing of Influenza Virus and SARS-CoV-2. *ACS Omega* **2021**, *6*, 6643–6653.
- (12) Deysher, G.; Shuck, C. E.; Hantanasirisakul, K.; Frey, N. C.; Foucher, A. C.; Maleski, K.; Sarycheva, A.; Shenoy, V. B.; Stach, E. A.; Anasori, B.; Gogotsi, Y. Synthesis of Mo₄VAIC₄ MAX Phase and Two-Dimensional Mo₄VC₄ MXene with Five Atomic Layers of Transition Metals. *ACS Nano* **2020**, *14*, 204–217.
- (13) Lin, Z.; Zhuo, M.; Zhou, Y.; Li, M.; Wang, J. Microstructures and Theoretical Bulk Modulus of Layered Ternary Tantalum Aluminum Carbides. *J. Am. Ceram. Soc.* **2006**, *89*, 3765–3769.
- (14) Zhang, J.; Liu, B.; Wang, J.; Zhou, Y. Low-Temperature Instability of Ti₂SnC: A Combined Transmission Electron Microscopy, Differential Scanning Calorimetry, and X-Ray Diffraction Investigations. *J. Mater. Res.* **2009**, *24*, 39–49.
- (15) Zhu, J.; Wang, M.; Lyu, M.; Jiao, Y.; Du, A.; Luo, B.; Gentle, I.; Wang, L. Two-Dimensional Titanium Carbonitride Mxene for High-Performance Sodium Ion Batteries. *ACS Appl. Nano Mater.* **2018**, *1*, 6854–6863.
- (16) Anasori, B.; Lukatskaya, M. R.; Gogotsi, Y. 2D Metal Carbides and Nitrides (MXenes) for Energy Storage. *Nat. Rev. Mater.* **2017**, *2*, 16098.
- (17) Ghidui, Y.; Lukatskaya, M.; Zhao, M.; Gogotsi, Y.; Barsoum, M. Conductive Two-Dimensional Titanium Carbide ‘Clay’ with High Volumetric Capacitance. *Nature* **2014**, *516*, 78–81.
- (18) Halim, J.; Cook, K. M.; Naguib, M.; Eklund, P.; Gogotsi, Y.; Rosen, J.; Barsoum, M. W. X-Ray Photoelectron Spectroscopy of Select Multi-Layered Transition Metal Carbides (MXenes). *Appl. Surf. Sci.* **2016**, *362*, 406–417.
- (19) Ibragimova, R.; Puska, M. J.; Komsa, H.-P. pH-Dependent Distribution of Functional Groups on Titanium-Based MXenes. *ACS Nano* **2019**, *13*, 9171–9181.
- (20) Yu, X.; Cai, X.; Cui, H.; Lee, S. W.; Yu, X. F.; Liu, B. Fluorine-Free Preparation of Titanium Carbide MXene Quantum Dots with High Near-Infrared Photothermal Performances for Cancer Therapy. *Nanoscale* **2017**, *9*, 17859–17864.

-
- (21) Seredych, M.; Maleski, K.; Mathis, T. S.; Gogotsi, Y. Delamination of MXenes using Bovine Serum Albumin. *Colloids Surf. A: Physicochem. Eng. Asp.* **2022**, *641*, 128580.
- (22) Kamysbayev, V.; Filatov, A. S.; Hu, H.; Rui, X.; Lagunas, F.; Wang, D.; Klie, R. F.; Talapin, D. V. Covalent Surface Modifications and Superconductivity of Two-Dimensional Metal Carbide MXenes. *Science* **2020**, *369*, 979–983.
- (23) Sokol, M.; Natu, V.; Kota, S.; Barsoum, M. W. On the Chemical Diversity of the MAX Phases. *Trends Chem.* **2019**, *1*, 210–223.
- (24) Ingason, A. S.; Petruhins, A.; Rosen, J. Toward Structural Optimization of MAX Phases as Epitaxial Thin Films. *Mater. Res. Lett.* **2016**, *4*, 152–160.
- (25) Eklund, P.; Rosen, J.; Persson, P. O. Å. Layered Ternary $M_{n+1}AX_n$ Phases and their 2D Derivative MXene: An Overview from a Thin-Film Perspective. *J. Phys. D: Appl. Phys.* **2017**, *50*, 113001.
- (26) Azin, C.; Tunca, B.; Petruhins, A.; Xin, B.; Yildizhan, M.; Persson, P. O. Å.; Vleugels, J.; Lambrinou, K.; Rosen, J.; Eklund, P. Deposition of MAX Phase-Containing Thin Films from a $(Ti,Zr)_2AlC$ Compound Target. *Appl. Surf. Sci.* **2021**, *551*, 149370.
- (27) Högberg, H.; Eklund, P.; Emmerlich, J.; Birch, J.; Hultman, L. Epitaxial Ti_2GeC , Ti_3GeC_2 , and Ti_4GeC_3 MAX-Phase Thin Films Grown by Magnetron Sputtering. *J. Mater. Res.* **2005**, *20*, 779–782.
- (28) Gouveia, J. D.; Morales-García, Á.; Viñes, F.; Gomes, J. R. B.; Illas, F. Facile Heterogeneously Catalyzed Nitrogen Fixation by MXenes. *ACS Catal.* **2020**, *10*, 5049–5056.
- (29) Hampden-Smith, M. J.; Kudas, T. T.; Chemical Vapor Deposition of Metals: Part 1. An Overview of CVD Processes. *Chem. Vap. Deposition* **1995**, *1*, 1–23.
- (30) Jurado, A.; Morales-García, Á.; Viñes, F.; Illas, F. CO_2 Identifying the Atomic Layer Stacking of Mo_2C MXene by Probe Molecule Adsorption. *J. Phys. Chem. C* **2021**, *125*, 26808–26813.
- (31) Gouveia, J. D.; Morales-García, Á.; Viñes, F.; Illas, F.; Gomes, J. R. B. MXenes as Promising Catalysts for Water Dissociation. *Appl. Catal. B.: Environ.* **2020**, *260*, 118191.
- (32) Gouveia, J. D.; Viñes, F.; Illas, F.; Gomes, J. R. B. MXenes Atomic Layer Stacking Phase Transitions and their Chemical Activity Consequences. *Phys. Rev. Mater.* **2020**, *4*, 054003.

-
- (33) Kresse, G.; Joubert, D. From Ultrasoft Pseudopotentials to the Projector Augmented-Wave Method. *Phys. Rev. B* **1999**, *59*, 1758.
- (34) Perdew, J. P.; Burke, K.; Ernzerhof, M. Generalized Gradient Approximation Made Simple. *Phys. Rev. Lett.* **1996**, *77*, 3865.
- (35) Grimme, S.; Antony, J.; Ehrlich, S.; Krieg, H. A Consistent and Accurate *Ab Initio* Parametrization of Density Functional Dispersion Correction (DFT-D) for the 94 Elements H-Pu. *J. Chem. Phys.* **2010**, *132*, 154104.
- (36) Blöchl, P. E. Projector Augmented-Wave method. *Phys. Rev. B* **1994**, *50*, 17953.
- (37) Monkhorst, H. J.; Pack, J. D. Special Points for Brillouin-Zone Integrations. *Phys. Rev. B* **1976**, *13*, 5188.
- (38) Janthon, P.; Luo, S.; Kozlov, S. M.; Viñes, F.; Limtrakul, J.; Truhlar, D. G.; Illas, F. Bulk Properties of Transition Metals: A Challenge for the Design of Universal Density Functionals. *J. Chem. Theory Comput.* **2014**, *10*, 3832–3839.
- (39) Janthon, P.; Kozlov, S. M.; Viñes, F.; Limtrakul, J.; Illas, F. Establishing the Accuracy of Broadly Used Density Functionals in Describing Bulk Properties of Transition Metals. *J. Chem. Theory Comput.* **2013**, *9*, 1631–1640.
- (40) Vega, L.; Viñes, F. Generalized Gradient Approximation Adjusted to Transition Metals Properties: Key Roles of Exchange and Local Spin Density. *J. Comput. Chem.* **2020**, *41*, 2598–2603.
- (41) Henkelman, G.; Uberuaga, B. P.; Jónsson, H. A Climbing Image Nudged Elastic Band Method for Finding Saddle Points and Minimum Energy Paths. *J. Chem. Phys.* **2000**, *113*, 9901.
- (42) Henkelman, G.; Jónsson, H. A Dimer Method for Finding Saddle Points on High Dimensional Potential Surfaces Using Only First Derivatives. *J. Chem. Phys.* **1999**, *111*, 7010.
- (43) Li, L.; Zhao, S.; Luo, X.-J.; Zhang, H.-B.; Yu, Z.-Z. Smart MXene-Based Janus Films with Multi-Responsive Actuation Capability and High Electromagnetic Interference Shielding Performances. *Carbon* **2021**, *175*, 594–2602.
- (44) Zhao, S.; Li, L.; Zhang, H.-B.; Qian, B.; Luo, J.-Q.; Deng, Z.; Shi, S.; Russell, T. P.; Yu, Z.-Z. Janus MXene Nanosheets for Macroscopic Assemblies. *Mater. Chem. Front.* **2020**, *4*, 910–917.
- (45) Kim, S.; Gamallo, P.; Viñes, F.; Lee, J. Y.; Illas, F. Substrate-Mediated Single-Atom Isolation: Dispersion of Ni and La on γ -Graphyne. *Theor. Chem. Acc.* **2017**, *136*, 80.

-
- (46) Kim, S.; Ruiz Pugidollers, A.; Gamallo, P.; Viñes, F.; Lee, J. Y. Functionalization of γ -Graphyne by Transition Metal Adatoms. *Carbon* **2017**, *120*, 63–70.
- (47) Oschinski, H.; Morales-García, Á.; Illas, F. Interaction of First Row Transition Metals with M_2C ($M = Ti, Zr, Hf, V, Nb, Ta, Cr, Mo,$ and W) MXenes: A Quest for Single-Atom Catalysts. *J. Phys. Chem. C* **2021**, *125*, 2477–2484.
- (48) Morales-Salvador, R.; Gouveia, J. D.; Morales-García, Á.; Viñes, F.; Gomes, J. R. B.; Illas, F. Carbon Capture and Usage by MXenes. *ACS Catal.* **2021**, *11*, 11248–11255.
- (49) Tripa, C. E.; Zubkov, T. S.; Yates Jr., J. T. N_2 Chemisorption on Stepped Pt Surfaces. Control by 2-D and 1-D Precursor Behavior. *J. Phys. Chem. B* **2001**, *105*, 3724–3732.
- (50) Levy, R. B.; Boudart, M. Platinum-Like Behavior of Tungsten Carbide in Surface Catalysis. *Science* **1973**, *181*, 547–549.
- (51) Atkins, P.; de Paula, J.; Keeler, J. Atkins' Physical Chemistry 11th Edition. Oxford University Press: Oxford, **2018**; pp 544.
- (52) Morales-García, Á.; Mayans, M.; Viñes, F.; Illas, F. Thickness biased capture of CO_2 on carbide MXenes. *Phys. Chem. Chem. Phys.* **2019**, *21*, 23136–23142.
- (53) Hannagan, R.T.; Giannakakis, G.; Flytzani-Stephanopoulos, M.; Sykes, E.C.H. Single-Atom Alloy Catalysis. *Chem. Rev.* **2020**, *120*, 12044–12088.
- (54) Manadé, M.; Viñes, F.; Illas, F. Transition Metal Adatoms on Graphene: A Systematic Density Functional Study. *Carbon* **2015**, *95*, 525–534.
- (55) Urbankowski, P.; Anasori, B.; Makaryan, T.; Er, D.; Kota, S.; Walsh, P. L.; Zhao, M.; Shenoy, V. B.; Barsoum, M. W.; Gogotsi, Y. Synthesis of Two-Dimensional Titanium Nitride Ti_4N_3 (MXene). *Nanoscale* **2016**, *8*, 11385–11391.
- (56) Dolz, D.; Morales-García, Á.; Viñes, F.; Illas, F. Exfoliation Energy as a Descriptor of MXenes Synthesizability and Surface Chemical Activity. *Nanomaterials* **2021**, *11*, 127.
- (57) Wong, Z. M.; Tan, T. L.; Tieu, A. J. K.; Yang, S.-W.; Xu, G. Q. Computational Discovery of Transparent Conducting In-Plane Ordered MXene (*i*-MXene) Alloys. *Chem. Mater.* **2019**, *31*, 4124–4132.
- (58) Wong, Z. M.; Deng, T.; Shi, W.; Wu, G.; Tan, T. L.; Yang, S.-W. High Performance Photocatalytic and Thermoelectric Two-Dimensional Asymmetrically Ordered Janus-like MXene Alloys. *Mater. Adv.* **2020**, *1*, 1176–1185.

-
- (59) Ougherb, C.; Ouahrani, T.; Badawi, M.; Morales-García, Á. Effect of the Sulfur Termination on the Properties of Hf₂CO₂ MXene. *Phys. Chem. Chem. Phys.* **2022**, *24*, 7243–7252.
- (60) Mishra, A.; Srivastava, P.; Carreras, A.; Tanaka, I.; Mizuseki, H.; Lee, K.-R.; Singh, A. K. Atomistic Origin of Phase Stability in Oxygen-Functionalized MXene: A Comparative Study. *J. Phys. Chem. C* **2017**, *121*, 18947–18953.
- (61) Yorulmaz, U.; Demiroğlu, I.; Çakir, D.; Gülseren, O.; Sevik, C. A Systematical *Ab-Initio* Review of Promising 2D MXene Monolayers towards Li-Ion Battery Applications. *J. Phys. Energy* **2020**, *2*, 032006.
- (62) Togo, A.; Tanaka, I. First Principles Phonon Calculations in Materials Science. *Scr. Mater.* **2015**, *108*, 1–5.
- (63) Tan, T. L.; Jin, H. M.; Sullivan, M. B.; Anasori, B.; Gogotsi, Y. High-Throughput Survey of Ordering Configurations in MXene Alloys Across Compositions and Temperatures. *ACS Nano* **2017**, *11*, 4407–4418.

Table of Contents

